Global and Planetary Change 223 (2023) 104078

Contents lists available at ScienceDirect

Global and Planetary Change

journal homepage: www.elsevier.com/locate/gloplacha

High altitude Pliocene to Pleistocene vegetation and climate change of the Kunlun Pass Basin, NE Tibetan Plateau

Florian Schwarz [a], Ulrich Salzmann [a,*], Feng Cheng [b,c], Jian Ni [d], Junsheng Nie [e], Megan R. Patchett [a], Xiangzhong Li [f], Lin Li [g], John Woodward [a], Carmala Garzione [c,g]

[a] Department of Geography and Environmental Sciences, Northumbria University, Newcastle upon Tyne, United Kingdom
[b] Key Laboratory of Orogenic Belts and Crustal Evolution, Ministry of Education, School of Earth and Space Sciences, Peking University, Beijing 100871, China
[c] Department of Earth and Environmental Sciences, University of Rochester, Rochester, NY, USA
[d] College of Life Sciences, Zhejiang Normal University, Jinhua, China
[e] Key Laboratory of Western China's Environmental System, College of Earth and Environmental Sciences, Lanzhou University, Lanzhou, China
[f] Yunnan Key Laboratory of Earth System Science, Yunnan University, Kunming 650500, China
[g] Department of Geosciences, College of Science, University of Arizona, Tucson, AZ 85721, USA

ARTICLE INFO

Editor: Howard Falcon-Lang

Keywords:
Pollen
Pliocene
Pleistocene
Tibetan Plateau
Semi-desert
Permafrost

ABSTRACT

The world largest alpine permafrost region, the Tibetan Plateau, will experience amplified warming under global climate change scenarios. Studying its environmental evolution in the geological past is crucial to further our understanding of mechanism and thresholds of climate change. Here we present a 3.5-million-year-long, high-altitude vegetation and climate record from the Kunlun Pass Basin to reconstruct the transition from the sustained warm, high carbon dioxide environment of the Pliocene to the cool glacial and interglacial periods of the Pleistocene, 4.31 to 0.85 million years (Ma) ago. The Early Pliocene pollen record indicates the occurrence of patches of broadleaved and coniferous forests in a semi-desert shrubland at this high-altitude site. Pollen derived quantitative climate estimates based on modern pollen rain transfer functions suggest a moister climate before 4.0 Ma with mean annual temperatures (MATs) > 14 °C warmer than today. The retreat of broadleaved and coniferous forests from the Kunlun Pass Basin area is linked to stepwise cooling at ~4.0 Ma and during the Plio-Pleistocene transition between 2.7 and 2.6 Ma. Pollen derived climate estimates and Δ_{47}-palaeothermometry indicate an abrupt cooling of ~4–8 °C resulting in the onset of permafrost condition on the Tibetan Plateau after 2.7 Ma. An expansion of Chenopodioideae dominated xerophytic shrublands after 3.8 Ma and 2.15 Ma indicates a reduction in precipitation on the NE Tibetan Plateau, which appears to be linked to a weakening of the East Asian Summer Monsoon at the Plio-Pleistocene transition. The reconstructed cooling at the Kunlun Pass Basin site reflects the regional expression of global climate change with high-elevation temperature amplification hence rejecting the notion of a major tectonic uplift of the Tibetan Plateau during the Plio-Pleistocene.

1. Introduction

Over the past 5 million years (Ma) the Earth underwent a major transition from the warm climates of the Pliocene to the Pleistocene ice ages. The cooling, which was primarily triggered by a combination of favourable astronomical forcing and declining atmospheric carbon dioxide concentrations (Maslin et al., 1998), led to the intensification of Northern Hemisphere Glaciation (NHG) at the Plio-Pleistocene transition. Over the last decades the Pliocene (5.3–2.6 Ma) has received particular scientific attention since it was the last geological Epoch with significantly higher than pre-industrial atmospheric carbon dioxide concentrations (pCO_2) of up to 365–415 ppm (Pagani et al., 2010) and global annual temperatures which exceeded the modern average by 2–4 °C (Brierley et al., 2009; Haywood et al., 2009; Martinez-Boti et al., 2015). However, the increased temperatures were not evenly distributed, and amplified warming during the late Pliocene (Piacenzian) of up to 19 °C has been reconstructed for the Northern Hemisphere high latitudes (Ballantyne et al., 2010; Panitz et al., 2016; Salzmann et al., 2013). Modell simulations suggest that high mountain ranges might experience similar amplified temperature increases under a global warming scenario (Feng et al., 2014; Nogués-Bravo et al., 2007), leading to a replacement of tundra shrub vegetation on plateau areas (Feng

* Corresponding author.
E-mail address: Ulrich.Salzmann@northumbria.ac.uk (U. Salzmann).

https://doi.org/10.1016/j.gloplacha.2023.104078
Received 22 November 2022; Received in revised form 22 February 2023; Accepted 26 February 2023
Available online 5 March 2023

et al., 2014; Wang et al., 2011). The pronounced warming at higher elevations might be further amplified by the reduced snow cover and upward migration of vegetation causing a "greening" of the albedo (Pepin et al., 2015).

Here we present a 3.5 million-year-long, high-altitude pollen record from the Kunlun Pass Basin (KPB) on the Tibetan Plateau, the largest alpine permafrost region on the Earth. Recently published Pliocene lacustrine isotope records from the same site indicate a permafrost-free environment on the northern Tibetan Plateau prior to 2.7 Ma highlighting the sensibility of alpine permafrost to global warming (Cheng et al., 2022). The KPB pollen record provides new insights into high altitude palaeovegetation and palaeoclimate variability from the warm Early Pliocene (Zanclean) to the intensification of large-scale NHG during and after the Plio-Pleistocene transition (4.31 to 0.85 Ma). By providing palynology-based quantitative and semiquantitative temperature and precipitation estimates, this study will also contribute to the controversy on the timing of the tectonic uplift of the NE Tibetan Plateau during the Plio-Pleistocene.

2. Regional setting

The KPB (35°39′N, 94°03′E) is located in the Eastern Kunlun Mountains to the south of the Qaidam Basin (Fig. 1) at a modern elevation of 4700 to 5300 m above sea level (a.s.l.) The basin has been described as a pull-apart basin of Pliocene and Pleistocene age (Song et al., 2005a) resulting from left-lateral strike-slip faulting along the Kunlun Fault. The sediments of the KPB are of Pliocene and Quaternary origin (Song et al., 2005a) and grouped into the Kunlun Formation (3.58–2.69 Ma), Qiangtang Formation (2.58–0.78 Ma) and Wangkun Formation (0.78–0.5 Ma). These late Cenozoic sediments are unconformably underlain by Triassic sedimentary rocks (Song et al., 2005a). The Kunlun Formation contains conglomerates, the Qiangtang Formation contains siltstones and mudstones from lacustrine and alluvial fan delta deposits and the Wangkun Formation contains glacially formed tills with mixed breccia and poorly sorted gravel (Cui et al., 1998; Song et al., 2005a; Wang et al., 2008).

Most of the high KPB is located in the permafrost zone. Today's climate is characterised by very low mean annual temperatures (MATs) of − 6.4 °C, and low mean annual precipitation (MAP) rates of 225 mm/a. The day-time high temperature of the warmest summer month in the KPB remains below 10 °C, and temperature and precipitation, and consequently vegetation cover, vary significantly depending on the actual elevation and local climate conditions. Locally wetter areas in the basin are covered with cold meadow and steppes with Poaceae and Cyperaceae, whereas drier parts are covered by xerophytic *Artemisia* and Chenopodioideae shrubs or deserts (Wang et al., 2008).

3. Materials and methods

3.1. Stratigraphy and age model

The sampled KPB section is dominated by laminated dark grey calcareous mudstone interbedded with sparse greyish siltstone and sandstone (Cheng et al., 2022), that have been interpreted as lacustrine deposits (Li et al., 2014a; Song et al., 2005a). The age model (Fig. 2) is based on recorrelated magnetostratigraphy (Song et al., 2005a) and biostratigraphy (Li et al., 2014a) in combination with piecewise linear interpolation (Cheng et al., 2022). The depositional maximum and minimum age of the sampled section can be confidently asssigned to 4.31 and 0.85 Ma. The age model has also been further improved by spectral analysis of carbon and oxygen isotopes, as well as carbonate content records using untuned age model resolved orbital-scale variation. A detailed description of the stratigraphy and age model of the analysed sediment section can be found in Cheng et al. (2022).

3.2. Palynological analysis

170 samples were taken for palynological analysis spanning from 4.31 to 0.85 Ma. 15–20 g of sediment per sample were processed at Northumbria University using standard palynological methods, including treatment with HCl (10%), sieving (125 μm), HF (48%) two hot HCl (10%) washes and final sieving at 10 μm. Residues were mounted in silicon oil and counted at 400× magnification. Most samples have a total sum of pollen and spores between 150 and 350 grains. The sample resolution for the Pliocene part of the record is significantly higher (~ 12.8 ka) than the Pleistocene part (~ 92.0 ka) which showed a lower pollen concentration and higher count of degraded sporomorphs. Two tablets of *Lycopodium* spores (Batch-Nr. 3862) (Stockmarr, 1971) were added to calculate pollen concentrations. Pollen and spores in 153 samples have been identified using the Northumbria University pollen

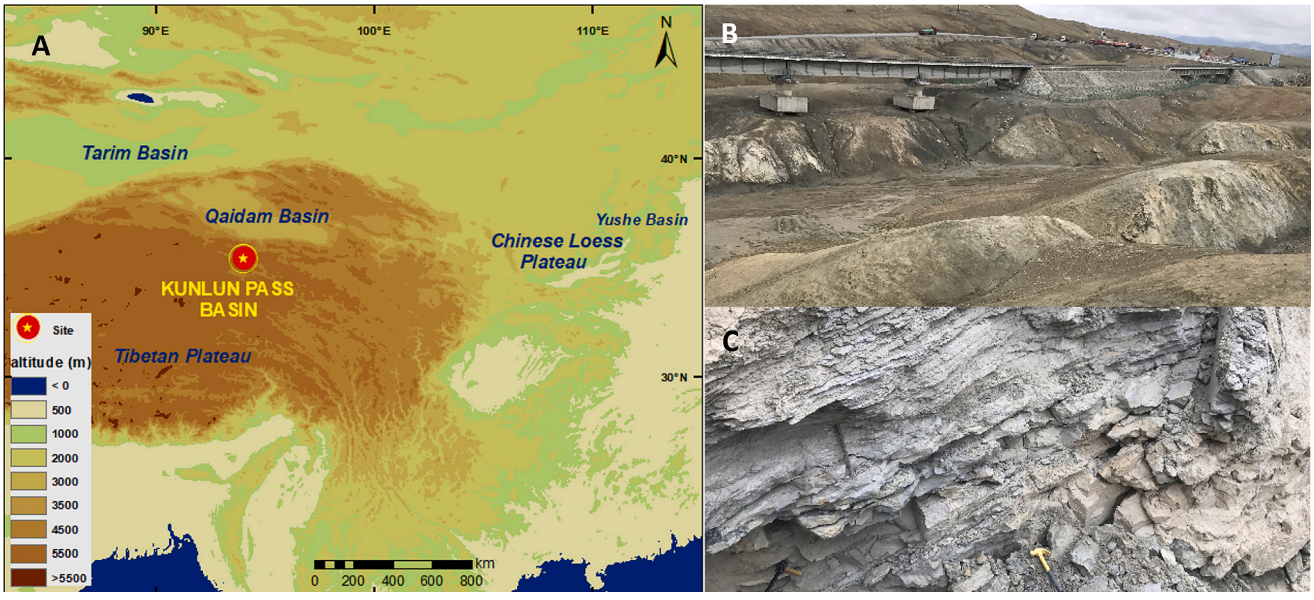

Fig. 1. A) Sampling site Kunlun Pass Basin (KPB) on the NE Tibetan Plateau (basemap: NOAA National Centers for Environmental Information, 2022); B) Outcrops of lacustrine deposits at KPB section; C) layered laminated dark grey calcareous mudstone of KPB section.

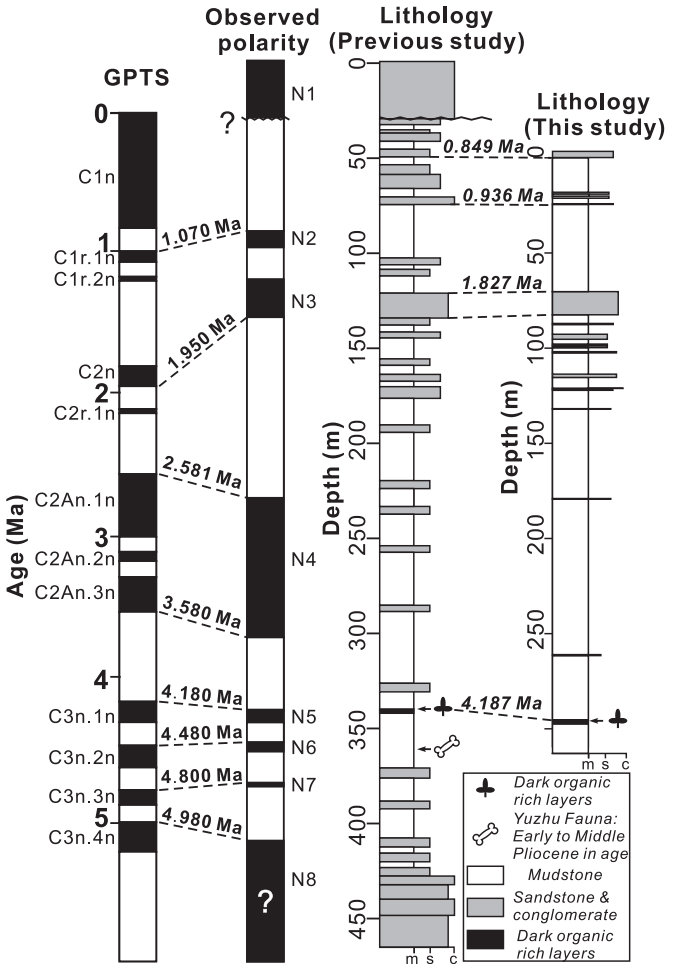

Fig. 2. Age model and stratigraphic column of the KPB section (Cheng et al., 2022). The magnetostratigraphy and biostratigraphy age constrains are from Li et al. (2014a) and Song et al. (2005a).

reference collection and literature (Beug, 2004; Demske et al., 2013; Kou et al., 2006; Li et al., 2014b). Pollen diagrams were produced with Tilia (Grimm, 1990). Pollen assemblage zones were defined following cluster analysis of CONISS (Grimm, 1987), leading to the establishment of 4 main and 12 subzones.

3.3. Principal component analysis

Principal component analysis (PCA) was conducted using R (R Core Team, 2020) in order to identify ecological groups and potential drivers of environmental change. The PCA was applied to all pollen taxa that exceeded 0.15% on average per sample. Prior to PCA, the pollen percentages were log transformed in order to account for very high individual taxa percentages, reduce the overall variance and emphasize the variability of lower percentage taxa (Marquer et al., 2014; Tonello and Prieto, 2008).

3.4. Pollen-based quantitative and semiquantitative climate reconstruction

We used the pollen ratios of *Artemisia*/Chenopodioideae (A/C) and *Artemisia*+Chenopodioideae/Cyperaceae (A+C/Cy) to semi-quantitively reconstruct Pliocene to Pleistocene temperature and precipitation changes. Modern pollen rain studies of lakes sediments on the Tibetan Plateau indicate a positive correlation between A/C and annual precipitation, whereas the A+C/Cy pollen ratio showed a significant correlation with July summer temperatures (Herzschuh, 2007; Zhang et al. 2018). *Artemisia* pollen percentages are high throughout most of the KPB record hence increasing the confidence of using A/C pollen ratios as qualitative indicators of precipitation (Koutsodendris et al., 2019).

In addition, we applied the weighted averaging-partial least squares (WA-PLS) regression to provide quantitative climate estimates. WA-PLS based transfer functions have been primarily applied to Quaternary samples, but the feasibility of this approach for deeper time intervals has been recently demonstrated by a Pliocene study from the neighbouring Qaidam Basin (Schwarz et al., 2022). Pollen-climate transfer functions use modern pollen-vegetation calibration datasets instead of presence-absence data and therefore provide in particular in semi-desert and mountainous regions substantial advantages over other quantitative approaches, such as the Coexistence Approach (Mosbrugger and Utescher, 1997; Utescher et al., 2014) or coexistence likelihood estimation (e.g. Harbert and Nixon, 2015). Recent data-model comparison studies also suggest that the presence-absence data-based nearest living relative methods tend to overestimate the cold winter temperature of the Pliocene high latitudes (Tindall et al., 2022).

Our pollen – climate transfer functions were trained with a modern pollen dataset of pollen assemblages from a total of 926 initial sample sites ranging from 74.5 to 104.17°E and 30.0 to 45.0°N based on the work of Ni et al. (2014) and Chen et al. (2010). After completing a modified homogenization process of the modern pollen dataset after Cao et al. (2013), the dataset was screened in multiple steps to improve the signal to noise ratio by removing low abundant taxa (Cao et al., 2014; Prentice, 1980) and to identify potential outlying samples, which could hamper an accurate establishment of the transfer functions. To ensure pollen compositions of the modern pollen training set are capable to reflect the fossil pollen assemblages, we excluded ambiguous taxa from our calculation with an unclear relationship between pollen percentages and climate variables, such as *Juglans/Pterocarya*, *Ilex*, *Solanum* and *Elaeagnus*. For the whole record, the pollen – climate transfer functions were able to cover between 88.7 and 100% of the total pollen sum (average: 97.8%), which points to a good reliability of the climate estimates with regards to taxa inclusions. Transfer functions for mean annual temperature (MAT), mean summer temperature (MST) and mean annual precipitation (MAP) were calculated based on square-root transformed pollen percentages using the package rioja (Juggins, 2009) in R (R Core Team, 2020). For a detailed description of the applied method and statistical results see Appendix 1 and Schwarz et al. (2022).

4. Results and discussion

4.1. Plant communities and their environmental controls

The KPB pollen record represents vegetation communities that prevailed under varying climatic conditions throughout the Plio-Pleistocene. PCA was used to investigate statistical relationships within the pollen dataset, in order to identify vegetation assemblages composed of co-occurring taxa with similar environmental preferences. The PCA diagram (Fig. 3) indicates a clear distinction between broad-leaved and coniferous, alpine steppes and meadows, shrub meadows and xerophytic shrubland. PCA axis 1 explains 15.5% of the total variance and separates the dry xerophytic shrublands from all other groups of pollen, suggesting precipitation as the controlling environmental forcing. PCA axis 2 explains 10.7% of the total variance separating, with declining PCA axis 2 values, alpine steppes and meadows from coniferous trees and alpine shrub meadows and broadleaved trees. This points to a temperature control with high PCA axis 2 values representing warmest conditions (Fig. 3).

Artemisia, Chenopodioideae, *Solanum* and *Ephedra* are typical representatives of temperate and alpine xerophytic shrublands. The relatively smaller ecological distance of *Artemisia* to other taxa of this group compared to Poaceae and Cyperaceae suggests that the pollen

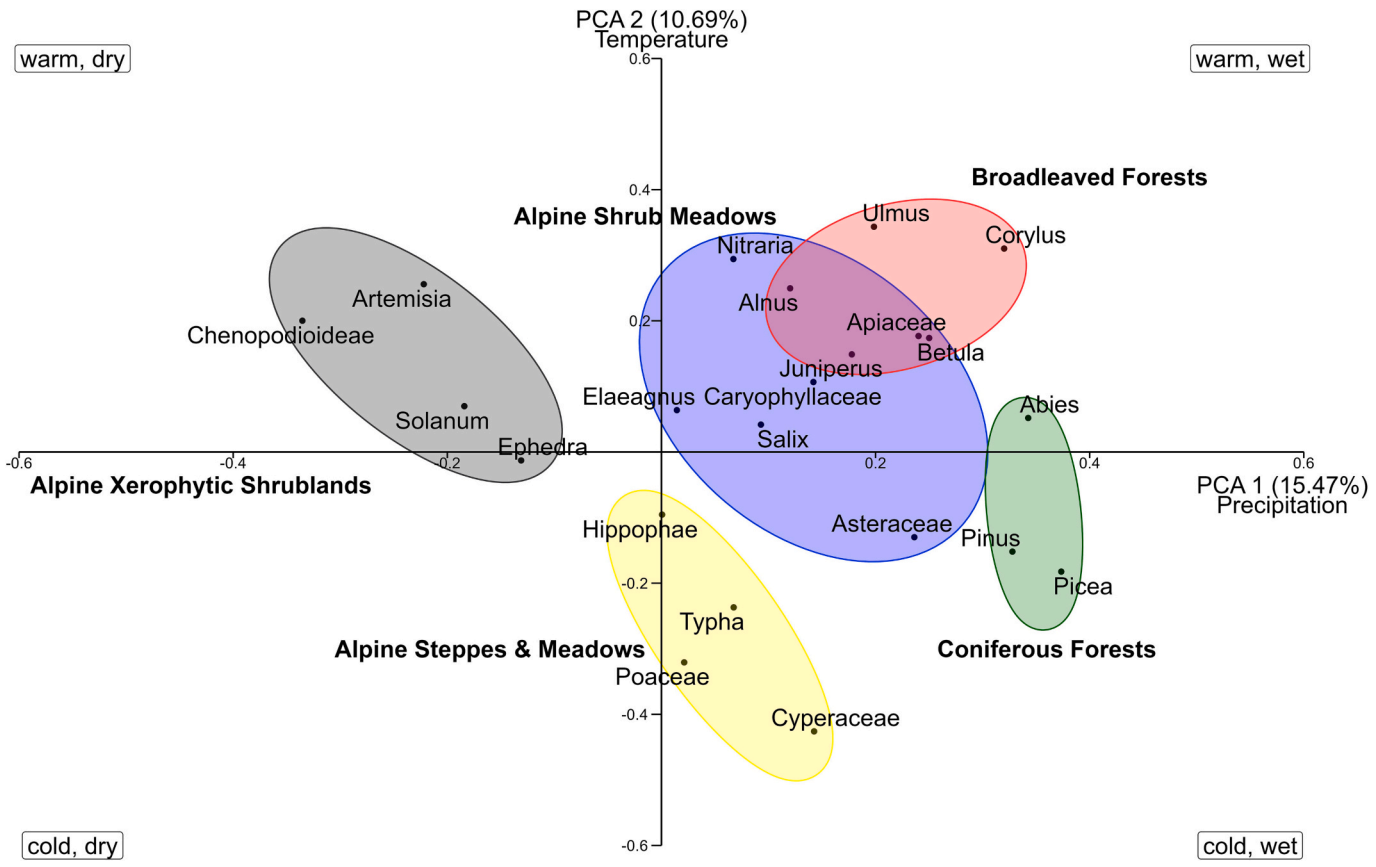

Fig. 3. PCA of the most abundant pollen taxa from the KPB record.

predominantly originates from very dry parts in the KPB area. Whereas the main broadleaved (*Betula*, *Alnus*, *Ulmus*, *Corylus*, *Salix*) and coniferous tree taxa (*Pinus*, *Picea*, *Juniperus*, *Abies*) can be assigned to forest and woodland communities, some of the most abundant herbs and shrubs, such as *Artemisia*, Asteraceae and Caryophyllaceae, can be components of both xerophytic shrublands or steppe communities on the Tibetan Plateau (Ni and Herzschuh, 2011; Zhao et al., 2012). The alpine shrub meadow group consists of *Salix*, *Juniperus*, *Elaeagnus*, Asteraceae, Apiaceae, Caryophyllaceae and *Nitraria*. In the modern Gongga Mountain (SE of KPB), *Salix* and *Juniperus* (*Sabina*) form alpine shrub meadows together with Poaceae and Cyperaceae, while Caryophyllaceae and Asteraceae are found in alpine sparse vegetation sites below the snowline (Li et al., 2012). Caryophyllaceae, Asteraceae and Apiaceae are found in abundance on the high Tibetan Plateau in wet locations (Yu et al., 2001). Although *Nitraria* is typically found in temperate semi-deserts in NW China, they can also inhabit wet sites with high water tables in mountainous areas (Cour et al., 1999; Yu et al., 2001; Zhao et al., 2007). *Elaeagnus* prefers normally drier and warmer parts in semi-deserts below 3200 m (Su et al., 2014), and as such, a closer ecological distance towards the xerophytic shrublands would have been expected. However, a record of fossil *Elaeagnus* leaves indicates the growth of this shrub at high altitudes (~3900 m) of the eastern Tibetan Plateau during the warmer Miocene (Su et al., 2014).

Poaceae and Cyperaceae most likely represent alpine steppes and meadows and not a local palaeo lakeshore vegetation. The very low abundances and partly missing presence of other aquatic plants, such as *Typha,* in the pollen record point to a reduced lakeshore vegetation or a reduced influx of local lakeshore pollen due to a large lake size (Vincens et al., 2005). Poaceae and Cyperaceae consistently have combined values of ~20–25% for most pollen zones in the KPB record, which is in good agreement with the modern vegetation on the Tibetan Plateau, where large parts of the central Tibetan Plateau are covered by alpine steppes and meadows (Ni, 2001; Ni and Herzschuh, 2011; Song et al., 2005b; Yu et al., 2001). Additionally, *Hippophae* can be assigned to this group. *Hippophae* often occurs on the Tibetan Plateau (Jia et al., 2012; Qiong et al., 2017; Su et al., 2014) in high altitude sites above the treeline together with grasses and sedges, and is able to withstand very cold temperatures (Li et al., 2005).

4.2. Pliocene to Pleistocene vegetation changes

4.2.1. Zanclean shrubs and open woodlands (Pollen Zone PZ 1)

Between 4.31 and 4.03 Ma the KPB was covered by xerophytic shrublands and alpine steppes and meadows with patches of open woodlands. Arboreal pollen reaches highest percentages (up to 27.2%) in this early interval of the record suggesting warmest temperatures (Fig. 4). The cool and cold-temperate mixed broadleaved and coniferous woodlands were composed of *Betula*, *Ulmus*, *Alnus*, *Elaeagnus*, *Salix, Juniperus, Pinus* and *Corylus* with some minor appearances of *Ilex* and *Juglans/Pterocarya*. The broadleaved and coniferous trees were possibly growing at habitat refugia with a warmer and wetter local climate. Given the extreme climate gradients in high mountain, the pollen signal might also reflect changes in the vegetation distribution along the altitudinal gradient.

Broadleaved tree pollen percentages decline at 4.16 and 4.03 Ma indicating a gradual change in the composition of the patchy broadleaved and conifer forests. Warm-temperate taxa such as *Ilex*, *Juglans/Pterocarya* and *Corylus* occur only rarely after 4 Ma, whereas taxa capable to survive colder conditions such as *Betula*, *Alnus*, *Salix* (tree/shrub), *Juniperus* (tree/shrub) and *Ulmus* remain. After 4.16 Ma (PZ 1-B), the broadleaved forests were replaced by *Pinus-Picea* coniferous forest patches. Additionally, the composition of the shrublands changed from Chenopodioideae dominated xerophytic shrublands to Asteraceae and Caryophyllaceae dominated alpine shrub meadows, which favour colder

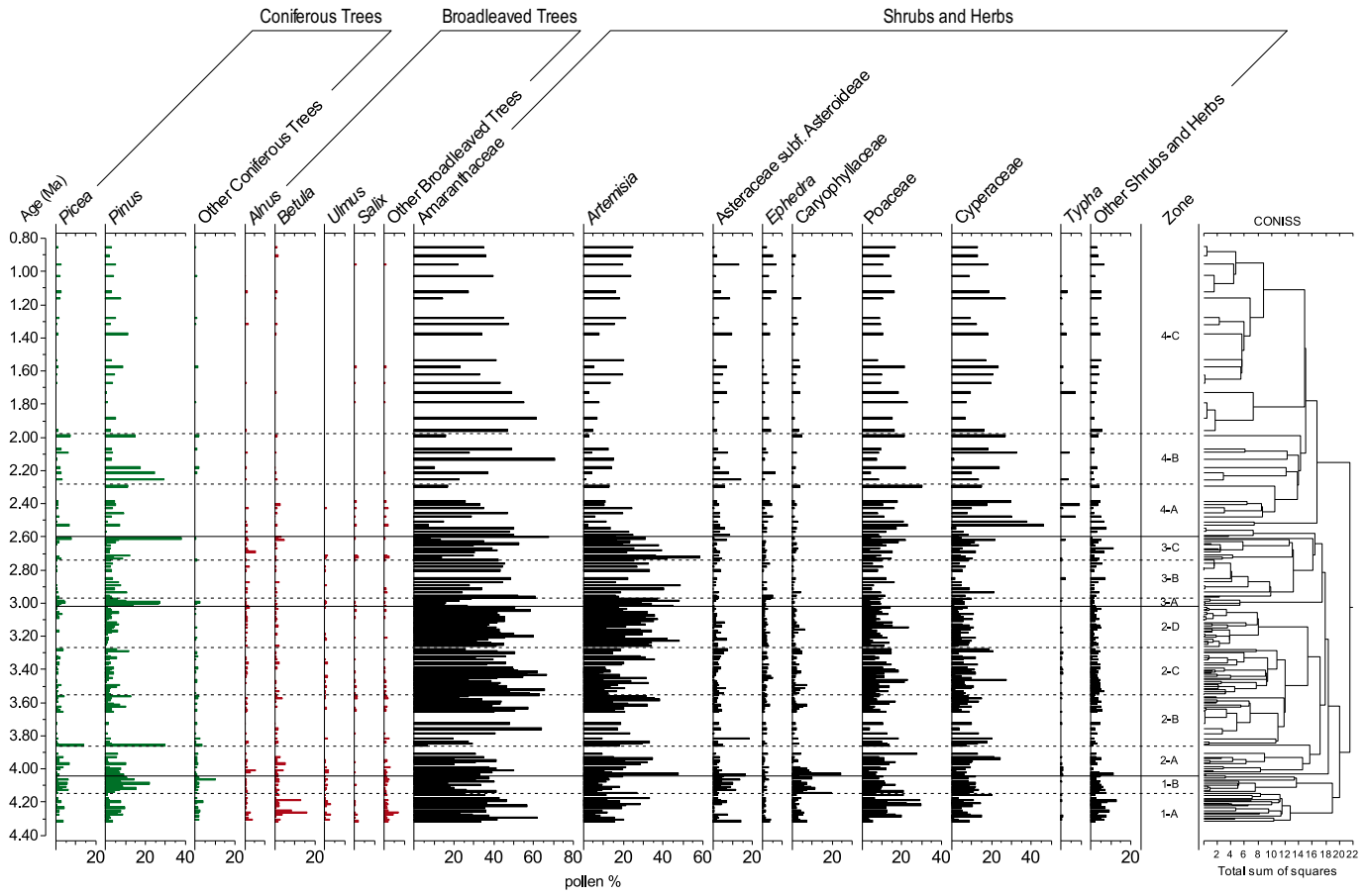

Fig. 4. Summary pollen percentage diagram of the KPB record.

and wetter conditions (Yu et al., 2001). These palaeovegetation changes indicate that the climate in the KPB became colder causing the retreat of broadleaved forest patches to warmer areas on the Tibetan Plateau and a downward shift of the broadleaved forest zone to lower altitudes.

Changes in the composition of broadleaved and coniferous forests were recorded across multiple other Zanclean study sites in China: Wang et al. (2006) shows that both coniferous and broadleaved forests existed in Xifeng, on the Chinese Loess Plateau (CLP), but that the forest composition and density changed drastically around 4.2 Ma. While *Pinus* still prevailed in the area, most of the broadleaved trees such as *Betula*, *Quercus* and *Juglans* became almost absent after ~4.0 to 3.8 Ma. An increase in the xerophytic shrubs Chenopodioideae and *Ephedra* indicates that between 4.2 and 4.0 Ma climate conditions became colder and drier. In Baode, northern CLP, broadleaved forests started to decline even earlier (~ 4.4 Ma) leading to the extinction of subtropical taxa (Li et al., 2011). In the Yushe Basin, climate cooling after 4.5 Ma caused a transition from subtropical to warm- temperate broadleaved forests (Shi et al., 1993). Between 4.3 and 4.1 Ma broadleaved forests declined and were replaced by coniferous forests (Shi et al., 1993), which coincide with vegetation changes recorded at the KPB.

4.2.2. Piacenzian xerophytic shrublands (PZ 2 and PZ 3)

After 4.03 Ma the patchy coniferous forest vegetation was largely replaced by alpine steppes and meadows and subsequently xerophytic shrublands (Fig. 4). The alpine steppe/meadow vegetation in the KPB area persisted until ~3.8 Ma and was characterised by high abundances in Poaceae, Cyperaceae and *Artemisia* besides some scattered coniferous forest trees that were still growing in this area. The transition from coniferous tree dominated open woodland to steppe/meadow vegetation with minor (except for one sample) appearances of coniferous trees marks a further cooling.

After 3.8 Ma, the KPB area experienced a strong expansion of Chenopodioideae dominated xerophytic shrublands, indicating the onset of a drier climate. *Artemisia* and Chenopodioideae consistently exceed 45% of the total pollen sum between ~3.8 Ma to 2.6 Ma, and their ratio (*Artemisia*/Chenopodioideae; A/C) can therefore be applied as an indicator for changes in the moisture availability or semi-quantitative precipitation estimate (Zhao et al., 2012). The expansion of Chenopodioideae shrublands were not only characteristic for the KPB, but have also been recorded on the CLP and in the Yushe Basin (Li et al., 2011; Shi et al., 1993; Wang et al., 2006). Chenopodioideae shrublands increased strongly after ~4.4 Ma (Li et al., 2011) on the northern CLP and after ~3.8 Ma (Wang et al., 2006) on the southern CLP.

After 3.28 Ma (PZ 2-D), *Artemisia* progressively increased and became the dominant component of the xerophytic shrublands of the KPB. Very high A/C ratios occur at ca. 3 Ma and between 2.74 and 2.6 Ma (PZ 3), which coincide with increased arboreal pollen percentages pointing to a short return to wetter conditions. A prominent shift of *Artemisia* percentages at the beginning of the mid-Piacenzian Warm Period, ca. 3.26 Ma, has also been recorded in the Qaidam Basin (Fig. 1), suggesting higher monsoonal strength with increased moisture availability (Koutsodendris et al., 2019; Schwarz et al., 2022).

4.2.3. Pleistocene Chenopodioideae scrubs and alpine meadows (PZ 4)

The onset of the Pleistocene is marked by a sequence of vegetation changes in response to drying and rapid cooling on the KPB. The sharp decline in *Artemisia*, which already started at 2.7 Ma (PZ 3-C) and increase in Poaceae and Cyperaceae after 2.6 Ma (PZ 4-A) indicate the transition to a Chenopodioideae dominated shrubland followed by an expansion of alpine steppes and meadows. These changes are accompanied by a sustained decline in broadleaved trees suggesting a further cooling of this region. After 2 Ma (PZ 4-C) arboreal pollen occur only in

low numbers in the KPB sediments reflecting a constant influx through long distance transport only.

Intensified drying and cooling after 2.6 Ma was also recognised in the nearby Qaidam Basin, where A/C ratios and broadleaved trees decreased (Cai et al., 2012). On the CLP (Chaona), a sudden decrease in broadleaved trees and a simultaneous increase in herbaceous plants implies a rapid cooling and drying during Plio-Pleistocene transition (Wu et al., 2007).

After ca. 1.8 Ma, both A/C ratios and WA-PLS derived precipitation estimates indicate a return to wetter conditions culminating around the Mid-Pleistocene Transition, ca. 1.3–1.0 Ma ago (Fig. 5). Although a lower sample resolution limits a further climate interpretation of the KPB record on glacial-interglacial time scales, the Pleistocene rainfall estimates show many similarities with sedimentological, pollen and leaf-wax hydrogen isotope (δDwax) - based moisture availability reconstructions of the Qaidam Basin record (Herb et al., 2015; Koutsodendris et al., 2018, 2019). Here, the increased moisture availability has been linked to a stronger monsoon that, along with further cooling, supported an extended glaciation on the Tibetan Plateau after the Mid-Pleistocene transition (Koutsodendris et al., 2018).

4.3. Pollen and clumped isotope based Plio-Pleistocene climate estimates and the role of declining pCO_2

With averaged Zanclean MATs between ca 4–8 °C which fall to 0–2 °C before the onset of the Piacenzian, the quantitative temperature estimates derived from the two independent pollen and isotope proxies show for the pre-Quaternary a remarkably good match (Fig. 5). Both proxies indicate a stepwise fall in temperatures between 4.0 and 3.3 Ma and 2.7–2.6 Ma. The latter cooling step marks the onset of permafrost conditions on the Tibetan Plateau, which subsequently became the largest alpine permafrost region on the Earth today (Cheng et al., 2022). However, whereas the Δ_{47} palaeothermometer indicates an ~8.1 °C decrease in MATs at 2.7 Ma to a Pleistocene average of −6.4 °C (Cheng et al., 2022), the pollen estimated decline in MATs appears to be considerably smaller, averaging between 0 to −2 °C only. Even the lowest pollen derived Pleistocene MAT estimates are still ~3.5 to 2.5 °C warmer than the modern KPB MATs of ~ −6.1 °C. Since the modern pollen calibration dataset had only a few study sites included where present annual temperatures are below modern temperatures of the KPB, it seems likely that the temperature estimates for the much colder Pleistocene environments have a consistent warm bias due to past non-analogue climates (i.e. beyond the calibration range) and edge effects (Seppä et al., 2004; ter Braak et al., 1993).

However, it is unlikely that such edge effects impacted on the precipitation estimates as many pollen assemblages in the modern pollen calibration dataset are derived from study sites with drier as well as wetter conditions than the modern KPB. Based on these pollen-based interpretations, a relatively stable semi-desert climate prevailed on the KPB with MAP around 230 mm/a. Highest rainfall amounts ranging between 250 and 350 mm/a occurred during the end of the Zanclean around 4 Ma and a further decline in precipitation occurred at a. 2.15 Ma (Fig. 5).

Throughout the various cooling steps, atmospheric pCO_2 declined from ~420 ppm in the Early Pliocene, to below 200 ppm in the Pleistocene glacials (e.g., Bartoli et al., 2011; Martinez-Boti et al., 2015; Pagani et al., 2010). Changes in atmospheric pCO_2 have a direct impact on plant physiological processes and various studies suggest that the reduced pCO_2 during the Pleistocene glacials favoured plants that use C_4 photosynthetic pathways, such as sedges and many plants of the subfamily Chenopodioideae and promote an opening of landscapes and lowering of tree lines (e.g. Dupont et al., 2019; Jolly and Haxeltine, 1997; Prentice et al., 2017). At the KPB, the Pliocene to Pleistocene decline in pCO_2 might have had an impact on the recorded change in the altitudinal zonation of the tree line, and expansion of xerophytic Chenopodioideae dominated shrub lands and alpine meadows (with Cyperaceae). The potential impact of pCO_2 on vegetation increases uncertainties in our quantitative climate estimates. However, the close correlation between the independent plant- and clumped-isotope-based reconstructions suggests that temperature and precipitation changes were the major controlling factors of vegetation change. A high covariance of δ^{18}Oc and δ^{13}Cc throughout the section and increased mean grain size provide additional evidence for a rapid cooling and regional aridification at the KPB throughout the Plio-Pleistocene transition (Cheng et al., 2022).

4.4. Global climate cooling and East Asian Summer Monsoon (EASM) variability

The late Zanclean decline in temperature and precipitation in the KPB, has also been described for the CLP where pollen records indicate a large-scale decline of broadleaved forests between ca 4.5 to 4.0 Ma (Li et al., 2011; Wang et al., 2006), while fossil mollusc assemblages show a switch from thermo-humidophilous to meso-xerophilous communities. (Li et al., 2008; Wu et al., 2006). The late Zanclean temperature decrease is not confined to Chinese records, suggesting that the retreat of forests and development of steppe/meadow vegetation after 4 Ma reflect the response of the KPB vegetation to global cooling.

Marine oxygen isotope records from benthic foraminifera show a general cooling of deep ocean waters throughout the Pliocene with superimposed warmer and colder intervals (Lisiecki and Raymo, 2005; Williams et al., 2009; Zachos et al., 2001). The Zanclean marine isotope stage (MIS) Gi26 (ca. 4.15 Ma; Lisiecki and Raymo, 2005) and especially MIS Gi20 (ca. 4.0 Ma; Lisiecki and Raymo, 2005) mark strong cooling intervals, which coincide with the demise of broadleaved trees in the KPB (Fig. 5). Around 4 Ma, the formation of glaciers on Svalbard and the occurrence of sea ice on the Yermak Plateau suggest intensified Arctic cooling (Knies et al., 2014; Risebrobakken et al., 2016), and while there is some doubt about post-depositional effects on benthic oxygen isotopes, the ODP 642B record in the eastern Nordic Sea shows that MIS Gi20 was a very strong cooling interval, potentially even surpassing the intensity of the MIS M2 event (Risebrobakken et al., 2016). During this time interval, the sea surface temperatures (SST) in the eastern equatorial Pacific cold tongue (EEPCT) started to cool (Lawrence et al., 2006) following the shoaling of the thermocline between 4.8 and 4.0 Ma (Ford et al., 2012; Steph et al., 2010). Although the exact timing is not entirely clear, cooling of the EEPCT between 4.3 and 3.6 Ma also caused the initialisation of a west-east gradient of SST in the equatorial Pacific (Dekens et al., 2007; Lawrence et al., 2006; Steph et al., 2010). Weak zonal and meridional SST gradients in the Pacific during the Pliocene thermal optimum between 4.2 and 4.0 Ma led to substantially weaker Walker and Hadley circulations compared to modern-day, respectively, and a northward migration of Hadley cells by up to 7° (Brierley et al., 2009). As a result, precipitation decreased in the equator and southern East Asia region, while precipitation over the Tibetan Plateau and northern China increased. These climate modelling results are in good agreement with the reconstructed MAP estimates for the KPB, which are highest in the late Zanclean intervals of the record (Fig. 5).

Increasing zonal and meridional gradients across the Pacific after 4.0 Ma (Brierley et al., 2009; Steph et al., 2010) could be responsible for a further change in precipitation pattern over East Asia and the establishment of extensive xerophytic shrublands in the KPB around 3.8 Ma. The change in palaeovegetation corresponds to a strong decline of MAP estimates to a range between 100 and 300 mm and a decline in the A/C ratio (Fig. 5). Aridification around 3.8 to 3.6 Ma has also been recognised in other Chinese records: the sediment deposits and ostracod assemblages in Lake Qinghai suggest lake shallowing and shrinking (Fu et al., 2013; Lu et al., 2017), grain size and lithofacies changes indicate the transition of a deep or semi-deep to a semi-shallow lake in the NW Qaidam Basin (Lu et al., 2015), the appearance of cold-aridiphilous molluscs on the CLP suggest colder and drier climate conditions in northern China (Wu et al., 2006), the establishment of xerophytic

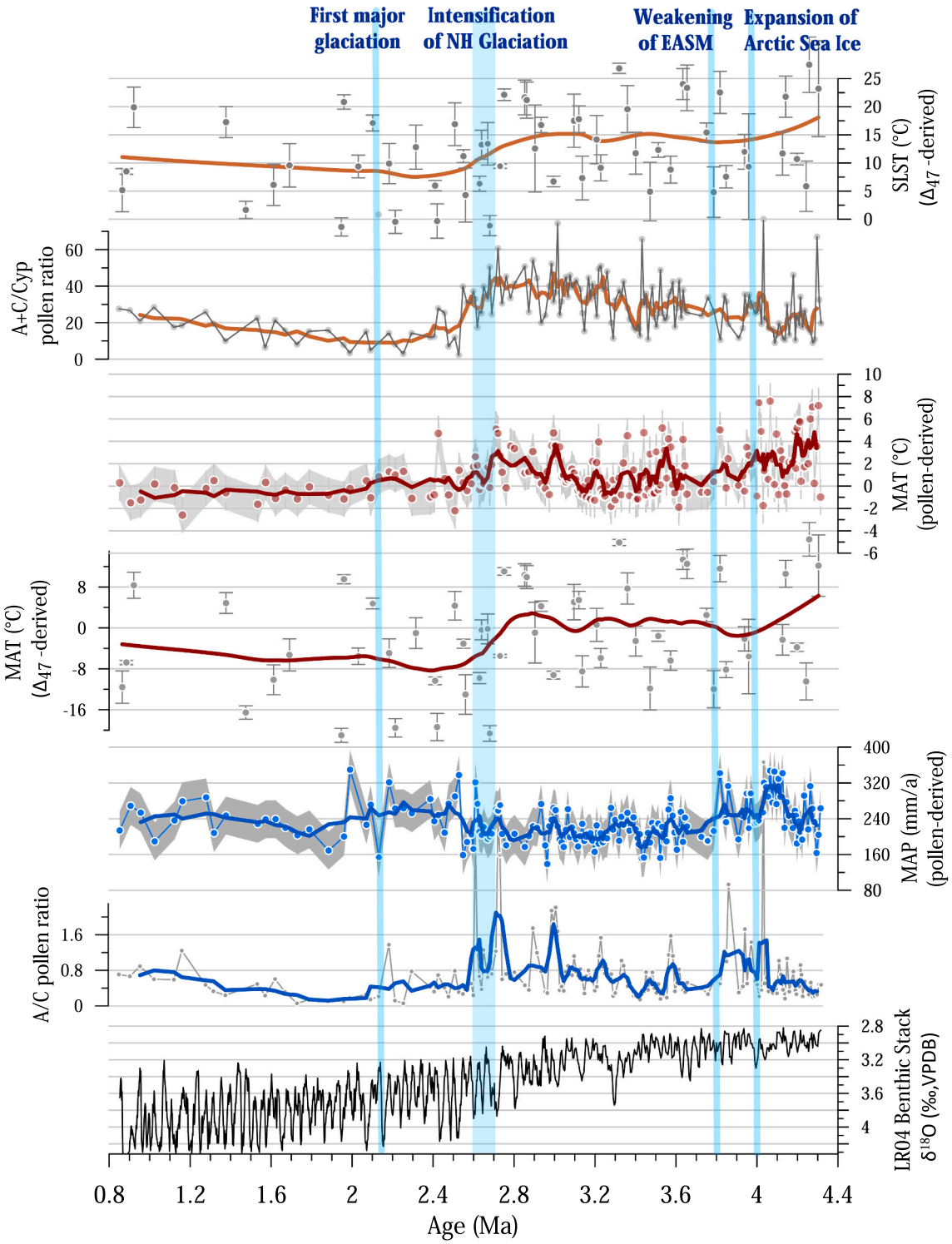

Fig. 5. Pollen-derived WA-PLS (this study) and clumped isotope (Δ_{47}) based (Cheng et al., 2022) palaeoclimate estimates from the KPB record. *Artemisia*/Chenopodioideae (A/C) ratio provide semi-quantitative estimates of annual precipitation. The sum of *Artemisia* and Chenopodioideae divided by Cyperaceae pollen percentages (A + C/Cyp) provides semi-quantitative estimates of the warmest month temperature to be compared with clumped isotope derived summer lake surface temperatures (SLST). Data curves have been smoothed using weighted average fit for pollen data and LOESS smooth for clumped isotopes. Blue bars mark regional and global cooling events: 4 Ma (MIS Gi20) - expansion of Arctic Sea Ice (Knies et al., 2014; Risebrobakken et al., 2016); 3.8 Ma - weakening of East Asian Monsoon (e.g. Fu et al., 2013; Lu et al., 2017); 2.7–2.6 Ma – intensification of Northern Hemisphere (NH) Glaciation (e.g. Bartoli et al., 2011); 2.15 Ma (MIS 82) – First major Pleistocene glaciation (Rohling et al., 2014). LR04 benthic oxygen isotope stack after Lisiecki and Raymo (2005). (For interpretation of the references to colour in this figure legend, the reader is referred to the web version of this article.)

shrublands on the CLP implies the advance of semi-deserts in northern China (Li et al., 2011; Wang et al., 2006). The hematite/goethite record from ODP Site 1143 in the South Chinese Sea indicates that in southern East Asia the summer monsoon was weaker from 4.0 to 3.8 Ma but stronger afterwards reaching wet conditions between 3.5 and 3.2 Ma (Ao et al., 2011). Based on the A/C ratio and reconstructed MAP estimates, the time period from 3.5 to 3.2 Ma was characterised by one of the driest intervals in the KPB, underpinning the divergence in monsoon evolution between southeastern and northwestern regions.

Between 3.2 and 2.7 Ma, the pollen- and isotope-based reconstructions as well as the A + C/Cyp ratio indicate a period of sustained higher MAT and summer temperatures. The timing of the vegetation and climate changes coincide with a period of increased pCO_2 between 3.2 and 2.7 Ma (Bartoli et al., 2011; Martinez-Boti et al., 2015; Pagani et al., 2010; Seki et al., 2010). Following the rapid cooling at ca. 2.7 Ma, which was accompanied by the intensification of the NHG, Pleistocene temperatures were consistently lower (Fig. 5). The pollen derived palaeoclimate estimates indicate a further decline in MATs and precipitation during the Pleistocene at MIS 82, 2.15 Ma ago (Fig. 5).

The reconstructed decrease in precipitation coincides with other regional sedimentological and palynological studies that suggested a weakening of the EASM for that time interval (Fu et al., 2013; Li et al., 2011; Lu et al., 2017; Wang et al., 2006). MIS 82 was significantly colder compared to the previous marine isotope stages (Hodell and Channell, 2016) and represents the first deep glaciation stage with a sea level low stand of ~70 m below present (Rohling et al., 2014). The steep drop in SST in the eastern equatorial Pacific (Lawrence et al., 2006) compared to the western equatorial Pacific (Wara et al., 2005) point to a very high zonal gradient, which is likely to be responsible for the decline in precipitation on the Tibetan Plateau and northern China around 2.15 Ma (Brierley et al., 2009).

4.5. Plio-Pleistocene tectonic evolution of the Kunlun Pass Basin

The Plio-Pleistocene tectonic evolution of the KPB has been subject to controversy. Previous studies suggest that the altitude of the KPB ranged from 400 to 4200 m during the Piacenzian (Cui et al., 1998; Wang and Chang, 2010; Wang et al., 2008; Wu et al., 2001) which is below its modern height of 4700 to 5300 m. The notion of a major uplift at the Plio-Pleistocene transition has been recently challenged by Cheng et al. (2022), who concluded that the ~8 °C at the KPB between 2.7 and 2.6 Ma (Fig. 5), indicated by clumped-isotopes, almost entirely reflects the regional expression of global climate change with high-elevation temperature amplification. The record therefore indicates for the northern Tibetan Plateau only a minor contribution of tectonic uplift to the recorded cooling (Cheng et al., 2022).

Our record of palaeovegetation and palaeoclimate change at the KPB supports the clumped isotope-based reconstructions by providing no indication for a major surface uplift between 4.31 and 0.85 Ma. The reconstructed strong cooling at 4.0 Ma, indicated by a decline in broadleaved trees on the KPB can also be observed in other Chinese vegetation records (Li et al., 2011; Wang et al., 2006), which were unaffected by tectonic movements. The second cooling event at the KPB site at ca. 2.6 Ma, can be confidently linked to the global cooling and intensification of the NHG at the Plio-Pleistocene transition. The expansion of sea ice formation in the Arctic (Knies et al., 2014; Risebrobakken et al., 2016) as well as the initiated cooling in the EEPCT (Lawrence et al., 2006; Steph et al., 2010) underline that the vegetation changes in the KPB were caused by global climate cooling and not tectonic uplift. Additionally, the high abundance of Caryophyllaceae in the early part of the record (especially PZ 1-B) indicates that the KPB was already uplifted to its modern height, since the modern occurrence of Caryophyllaceae is limited to high alpine sites (> 4000 m) on the Tibetan Plateau (Chen et al., 2010; Ni et al., 2014; Yu et al., 2001).

5. Conclusions

The 3.5 Ma long KPB record provides unique insights into the response of a high altitude semi-arid ecosystem to climate change. The fossil pollen assemblages indicate the persistence of semi-desert conditions and a stepwise decline in deciduous and needleleaf trees after 4 Ma followed, by expansion of *Artemisia*-Chenopodioideae shrubland and alpine meadows after 3.8 Ma and 2.7 Ma. These vegetation changes can be confidently attributed to regional aridification at 4.0, 3.8 and 2.15 Ma, and global cooling events at the onset of the Pliocene, which coincide with the intensification of NHG. The KPB record provides therefore no evidence for major tectonic uplift throughout the Piacenzian and Pleistocene. The excellent correlation between the independent pollen and clumped-isotope based proxies highlights the robustness of the WA-PLS based climate estimates for pre-Quaternary geological epochs, as long as they have been trained with a sufficient number of regional modern pollen rain measurements. With Early Pliocene MATs >14 °C warmer than today, the record provides multiple proxy evidence for amplified warming and permafrost free conditions at high-altitude regions of the Tibetan Plateau under high pCO2 concentrations that are similar to present day.

Declaration of Competing Interest

The authors declare that they have no known competing financial interests or personal relationships that could have appeared to influence the work reported in this paper.

Data availability

All palynological data and pollen-based climate estimates generated for this study are included in the Supplementary Information.

Acknowledgements

U.S. and J.N. acknowledge financial support from the Royal Society (IE141128). F.C. is supported by the National Science Foundation of China (U22B6002) and open grant from the Yunnan Key Laboratory of Earth Science (ESS2021001). C.G. is supported by U.S. NSF grants EAR-1348005 and OISE-1545859. Clumped instrumentation was supported by NSF EAR-0949191.

Appendix A. Supplementary data

Supplementary data to this article can be found online at https://doi.org/10.1016/j.gloplacha.2023.104078.

References

Ao, H., Dekkers, M.J., Qin, L., Xiao, G., 2011. An updated astronomical timescale for the Plio-Pleistocene deposits from South China Sea and new insights into Asian monsoon evolution. Quat. Sci. Rev. 30, 1560–1575. https://doi.org/10.1016/j.quascirev.2011.04.009.

Ballantyne, A.P., Greenwood, D.R., Sinninghe Damsté, J.S., Csank, A.Z., Eberle, J.J., Rybczynski, N., 2010. Significantly warmer Arctic surface temperatures during the Pliocene indicated by multiple independent proxies. Geology 38, 603–606. https://doi.org/10.1130/G30815.1.

Bartoli, G., Hönisch, B., Zeebe, R.E., 2011. Atmospheric CO2 decline during the Pliocene intensification of Northern Hemisphere glaciations. Paleoceanography 26. https://doi.org/10.1029/2010PA002055.

Beug, H.-J., 2004. Leitfaden der Pollenbestimmung für Mitteleuropa und angrenzende Gebiete, first ed. Dr. Friedrich Pfeil, Munich.

ter Braak, C., Juggins, S., Birks, H., van der Voet, H., 1993. Weighted Averaging Partial Least Squares regression (WA-PLS): Definition and comparison with other methods for species-environment calibration. In: Patil, G.P., Rao, C.R. (Eds.), Multivariate Environmental Statistics. Elsevier, Amsterdam, pp. 525–560.

Brierley, C.M., Fedorov, A.V., Liu, Z., Herbert, T.D., Lawrence, K.T., LaRiviere, J.P., 2009. Greatly Expanded Tropical warm Pool and Weakened Hadley Circulation in the early Pliocene. Science 323, 1714–1718. https://doi.org/10.1126/science.1167625.

Cai, M., Fang, X., Wu, F., Miao, Y., Appel, E., 2012. Pliocene–Pleistocene stepwise drying of Central Asia: Evidence from paleomagnetism and sporopollen record of the deep borehole SG-3 in the western Qaidam Basin, NE Tibetan Plateau. Glob. Planet. Chang. 94–95, 72–81. https://doi.org/10.1016/j.gloplacha.2012.07.002.

Cao, X.-Y., Ni, J., Herzschuh, U., Wang, Y.-B., Zhao, Y., 2013. A late Quaternary pollen dataset from eastern continental Asia for vegetation and climate reconstructions: Set up and evaluation. Rev. Palaeobot. Palynol. 194, 21–37. https://doi.org/10.1016/j.revpalbo.2013.02.003.

Cao, X.-Y., Herzschuh, U., Telford, R.J., Ni, J., 2014. A modern pollen–climate dataset from China and Mongolia: assessing its potential for climate reconstruction. Rev. Palaeobot. Palynol. 211, 87–96. https://doi.org/10.1016/j.revpalbo.2014.08.007.

Chen, Y., Ni, J., Herzschuh, U., 2010. Quantifying modern biomes based on surface pollen data in China. Glob. Planet. Chang. 74, 114–131. https://doi.org/10.1016/j.gloplacha.2010.09.002.

Cheng, F., Garzione, C., Li, X., Salzmann, U., Schwarz, F., Haywood, A.M., Tindall, J., Nie, J., Li, L., Wang, L., Abbott, B.W., Elliott, B., Liu, W., Upadhyay, D., Arnold, A., Tripati, A., 2022. Alpine permafrost could account for a quarter of thawed carbon based on Plio-Pleistocene paleoclimate analogue. Nat. Commun. 13, 1329. https://doi.org/10.1038/s41467-022-29011-2.

Cour, P., Zheng, Z., Duzer, D., Calleja, M., Yao, Z., 1999. Vegetational and climatic significance of modern pollen rain in northwestern Tibet. Rev. Palaeobot. Palynol. 104, 183–204. https://doi.org/10.1016/S0034-6667(98)00062-1.

Cui, Z., Wu, Y., Liu, G., 1998. Discovery and character of the Kunlun-Yellow River Movement. Chin. Sci. Bull. 43, 833–836. https://doi.org/10.1007/bf03182748.

Dekens, P.S., Ravelo, A.C., McCarthy, M.D., 2007. Warm upwelling regions in the Pliocene warm period. Paleoceanography 22. https://doi.org/10.1029/2006PA001394.

Demske, D., Tarasov, P.E., Nakagawa, T., 2013. Atlas of pollen, spores and further non-pollen palynomorphs recorded in the glacial-interglacial late Quaternary sediments of Lake Suigetsu, Central Japan. Quat. Int. 290-291, 164–238. https://doi.org/10.1016/j.quaint.2012.02.002.

Dupont, L.M., Caley, T., Castañeda, I.S., 2019. Effects of atmospheric CO2 variability of the past 800 kyr on the biomes of Southeast Africa. Clim. Past 15, 1083–1097. https://doi.org/10.5194/cp-15-1083-2019.

Feng, S., Hu, Q., Huang, W., Ho, C.-H., Li, R., Tang, Z., 2014. Projected climate regime shift under future global warming from multi-model, multi-scenario CMIP5 simulations. Glob. Planet. Chang. 112, 41–52. https://doi.org/10.1016/j.gloplacha.2013.11.002.

Ford, H.L., Ravelo, A.C., Hovan, S., 2012. A deep Eastern Equatorial Pacific thermocline during the early Pliocene warm period. Earth Planet. Sci. Lett. 355-356, 152–161. https://doi.org/10.1016/j.epsl.2012.08.027.

Fu, C., An, Z., Qiang, X., Bloemendal, J., Song, Y., Chang, H., 2013. Magnetostratigraphic determination of the age of ancient Lake Qinghai, and record of the East Asian monsoon since 4.63 Ma. Geology 41, 875–878. https://doi.org/10.1130/G34418.1.

Grimm, E.C., 1987. CONISS: a FORTRAN 77 program for stratigraphically constrained cluster analysis by the method of incremental sum of squares. Comput. Geosci. 13, 13–35. https://doi.org/10.1016/0098-3004(87)90022-7.

Grimm, E.C., 1990. Tilia and Tiliagraph. PC spreadsheet and graphics software for pollen data. INQUA. Work. Gr. Data-Handling Methods Newsl. 4, 5–7.

Harbert, R.S., Nixon, K.C., 2015. Climate reconstruction analysis using coexistence likelihood estimation (CRACLE): a method for the estimation of climate using vegetation. Am. J. Bot. 102, 1277–1289. https://doi.org/10.3732/ajb.1400500.

Haywood, A.M., Chandler, M.A., Valdes, P.J., Salzmann, U., Lunt, D.J., Dowsett, H.J., 2009. Comparison of mid-Pliocene climate predictions produced by the HadAM3 and GCMAM3 general circulation models. Glob. Planet. Chang. 66, 208–224. https://doi.org/10.1016/j.gloplacha.2008.12.014.

Herb, C., Appel, E., Voigt, S., Koutsodendris, A., Pross, J., Zhang, W., Fang, X., 2015. Orbitally tuned age model for the late Pliocene–Pleistocene lacustrine succession of drill core SG-1 from the western Qaidam Basin (NE Tibetan Plateau). Geophys. J. Int. 200, 35–51. https://doi.org/10.1093/gji/ggu372.

Herzschuh, U., 2007. Reliability of pollen ratios for environmental reconstructions on the Tibetan Plateau. J. Biogeogr. 34, 1265–1273. https://doi.org/10.1111/j.1365-2699.2006.01680.x.

Hodell, D.A., Channell, J.E.T., 2016. Mode transitions in Northern Hemisphere glaciation: co-evolution of millennial and orbital variability in Quaternary climate. Clim. Past 12, 1805–1828. https://doi.org/10.5194/cp-12-1805-2016.

Jia, D.R., Abbott, R.J., Liu, T.L., Mao, K.S., Bartish, I.V., Liu, J.Q., 2012. Out of the Qinghai-Tibet Plateau: evidence for the origin and dispersal of Eurasian temperate plants from a phylogeographic study of *Hippophaë rhamnoides* (Elaeagnaceae). New Phytol. 194, 1123–1133. https://doi.org/10.1111/j.1469-8137.2012.04115.x.

Jolly, D., Haxeltine, A., 1997. Effect of Low Glacial atmospheric CO2 on Tropical African Montane Vegetation. Science 276, 786–788. https://doi.org/10.1126/science.276.5313.786.

Juggins, S., 2009. Package 'rioja': Analysis of Quaternary Science Data. The Comprehensive R Archive Network. https://cran.r-project.org/package=rioja.

Knies, J., Cabedo-Sanz, P., Belt, S.T., Baranwal, S., Fietz, S., Rosell-Melé, A., 2014. The emergence of modern sea ice cover in the Arctic Ocean. Nat. Commun. 5, 5608. https://doi.org/10.1038/ncomms6608.

Kou, X.Y., Ferguson, D.K., Xu, J.X., Wang, Y.F., Li, C.S., 2006. The reconstruction of paleovegetation and paleoclimate in the late Pliocene of West Yunnan, China. Clim. Chang. 77, 431–448. https://doi.org/10.1007/s10584-005-9039-5.

Koutsodendris, A., Sachse, D., Appel, E., Herb, C., Fischer, T., Fang, X., Pross, J., 2018. Prolonged Monsoonal Moisture Availability Preconditioned Glaciation of the Tibetan Plateau during the Mid-Pleistocene transition. Geophys. Res. Lett. 45 (13) https://doi.org/10.1029/2018GL079303, 020-13,030.

Koutsodendris, A., Allstädt, F.J., Kern, O.A., Kousis, I., Schwarz, F., Vannacci, M., Woutersen, A., Appel, E., Berke, M.A., Fang, X., Friedrich, O., Hoorn, C., Salzmann, U., Pross, J., 2019. Late Pliocene vegetation turnover on the NE Tibetan Plateau (Central Asia) triggered by early Northern Hemisphere glaciation. Glob. Planet. Chang. 180, 117–125. https://doi.org/10.1016/j.gloplacha.2019.06.001.

Lawrence, K.T., Liu, Z., Herbert, T.D., 2006. Evolution of the Eastern Tropical Pacific through Plio-Pleistocene Glaciation. Science 312, 79–83. https://doi.org/10.1126/science.1120395.

Li, C., Yang, Y., Junttila, O., Palva, E.T., 2005. Sexual differences in cold acclimation and freezing tolerance development in sea buckthorn (*Hippophae rhamnoides* L.) ecotypes. Plant Sci. 168, 1365–1370. https://doi.org/10.1016/j.plantsci.2005.02.001.

Li, F., Rousseau, D.-D., Wu, N., Hao, Q., Pei, Y., 2008. Late Neogene evolution of the East Asian monsoon revealed by terrestrial mollusk record in Western Chinese Loess Plateau: from winter to summer dominated sub-regime. Earth Planet. Sci. Lett. 274, 439–447. https://doi.org/10.1016/j.epsl.2008.07.038.

Li, Q., Ge, Q.S., Tong, G.B., 2012. Modern pollen-vegetation relationship based on discriminant analysis across an altitudinal transect on Gongga Mountain, eastern Tibetan Plateau. Chin. Sci. Bull. 57, 4600–4608. https://doi.org/10.1007/s11434-012-5236-6.

Li, Q., Xie, G., Takeuchi, G.T., Deng, T., Tseng, Z.J., Grohé, C., Wang, X., 2014a. Vertebrate fossils on the roof of the world: Biostratigraphy and geochronology of high-elevation Kunlun Pass Basin, northern Tibetan Plateau, and basin history as related to the Kunlun strike-slip fault. Palaeogeogr., Palaeoclimatol. Palaeoecol. 411, 46–55. https://doi.org/10.1016/j.palaeo.2014.06.029.

Li, S.-P., Li, J.-F., Ferguson, D.K., Wang, N.-W., He, X.-X., Yao, J.-X., 2014b. Palynological analysis of the late early Pleistocene sediments from Queque Cave in Guangxi, South China. Quat. Int. 354, 24–34. https://doi.org/10.1016/j.quaint.2014.01.053.

Li, X.R., Fang, X.M., Wu, F.L., Mia, Y.F., 2011. Pollen evidence from Baode of the northern Loess Plateau of China and strong East Asian summer monsoons during the early Pliocene. Chin. Sci. Bull. 56, 64–69. https://doi.org/10.1007/s11434-010-4235-8.

Lisiecki, L.E., Raymo, M.E., 2005. A Pliocene-Pleistocene stack of 57 globally distributed benthic δ18O records. Paleoceanography 20, 1–17. https://doi.org/10.1029/2004PA001071.

Lu, F., An, Z., Chang, H., Dodson, J., Qiang, X., Yan, H., Dong, J., Song, Y., Fu, C., Li, X., 2017. Climate change and tectonic activity during the early Pliocene warm period from the ostracod record at Lake Qinghai, northeastern Tibetan Plateau. J. Asian Earth Sci. 138, 466–476. https://doi.org/10.1016/j.jseaes.2017.02.031.

Lu, Y., Fang, X.M., Appel, E., Wang, J.Y., Herb, C., Han, W.X., Wu, F.L., Song, C.H., 2015. A 7.3-1.6 Ma grain size record of interaction between anticline uplift and climate change in the western Qaidam Basin, NE Tibetan Plateau. Sediment. Geol. 319, 40–51. https://doi.org/10.1016/j.sedgeo.2015.01.008.

Marquer, L., Gaillard, M.-J., Sugita, S., Trondman, A.-K., Mazier, F., Nielsen, A.B., Fyfe, R.M., Odgaard, B.V., Alenius, T., Birks, H.J.B., Bjune, A.E., Christiansen, J., Dodson, J., Edwards, K.J., Giesecke, T., Herzschuh, U., Kangur, M., Lorenz, S., Poska, A., Schult, M., Seppä, H., 2014. Holocene changes in vegetation composition in northern Europe: why quantitative pollen-based vegetation reconstructions matter. Quat. Sci. Rev. 90, 199–216. https://doi.org/10.1016/j.quascirev.2014.02.013.

Martinez-Boti, M.A., Foster, G.L., Chalk, T.B., Rohling, E.J., Sexton, P.F., Lunt, D.J., Pancost, R.D., Badger, M.P.S., Schmidt, D.N., 2015. Plio-Pleistocene climate sensitivity evaluated using high-resolution CO2 records. Nature 518, 49–54. https://doi.org/10.1038/nature14145.

Maslin, M.A., Li, X.S., Loutre, M.F., Berger, A., 1998. The contribution of orbital forcing to the progressive intensification of the Northern Hemisphere Glaciation. Quat. Sci. Rev. 17, 411–426. https://doi.org/10.1016/S0277-3791(97)00047-4.

Mosbrugger, V., Utescher, T., 1997. The coexistence approach—a method for quantitative reconstructions of Tertiary terrestrial palaeoclimate data using plant fossils. Palaeogeogr. Palaeoclimatol. Palaeoecol. 134, 61–86. https://doi.org/10.1016/S0031-0182(96)00154-X.

Ni, J., 2001. A biome classification of China based on plant functional types and the BIOME3 model. Folia Geobot. 36, 113–129. https://doi.org/10.1007/bf02803157.

Ni, J., Herzschuh, U., 2011. Simulating Biome distribution on the Tibetan Plateau using a modified global vegetation model. Arct. Antarct. Alp. Res. 43, 429–441. https://doi.org/10.1657/1938-4246-43.3.429.

Ni, J., Cao, X., Jeltsch, F., Herzschuh, U., 2014. Biome distribution over the last 22,000yr in China. Palaeogeogr. Palaeoclimatol. Palaeoecol. 409, 33–47. https://doi.org/10.1016/j.palaeo.2014.04.023.

NOAA National Centers for Environmental Information, 2022. Digital Elevation Models Global Mosaic (Elevation Values). https://gis.ngdc.noaa.gov/arcgis/rest/services/DEM_mosaics/DEM_global_mosaic/ImageServer/ (accessed 14 November 2022).

Nogués-Bravo, D., Araújo, M.B., Errea, M.P., Martínez-Rica, J.P., 2007. Exposure of global mountain systems to climate warming during the 21st Century. Glob. Environ. Chang. 17, 420–428. https://doi.org/10.1016/j.gloenvcha.2006.11.007.

Pagani, M., Liu, Z., LaRiviere, J., Ravelo, A.C., 2010. High Earth-system climate sensitivity determined from Pliocene carbon dioxide concentrations. Nat. Geosci. 3, 27–30. https://doi.org/10.1038/ngeo724.

Panitz, S., Salzmann, U., Risebrobakken, B., De Schepper, S., Pound, M.J., 2016. Climate variability and long-term expansion of peatlands in Arctic Norway during the late Pliocene (ODP Site 642, Norwegian Sea). Clim. Past 12, 1043–1060. https://doi.org/10.5194/cp-12-1043-2016.

Pepin, N., Bradley, R.S., Diaz, H.F., Baraer, M., Caceres, E.B., Forsythe, N., Fowler, H., Greenwood, G., Hashmi, M.Z., Liu, X.D., Miller, J.R., Ning, L., Ohmura, A., Palazzi, E., Rangwala, I., Schöner, W., Severskiy, I., Shahgedanova, M., Wang, M.B., Williamson, S.N., Yang, D.Q., 2015. Elevation-dependent warming in mountain

regions of the world. Nat. Clim. Chang. 5, 424. https://doi.org/10.1038/nclimate2563.
Prentice, I.C., 1980. Multidimensional scaling as a research tool in Quaternary palynology: a review of theory and methods. Rev. Palaeobot. Palynol. 31, 71–104. https://doi.org/10.1016/0034-6667(80)90023-8.
Prentice, I.C., Cleator, S.F., Huang, Y.H., Harrison, S.P., Roulstone, I., 2017. Reconstructing ice-age palaeoclimates: Quantifying low-CO2 effects on plants. Glob. Planet. Chang. 149, 166–176. https://doi.org/10.1016/j.gloplacha.2016.12.012.
Qiong, L., Zhang, W., Wang, H., Zeng, L., Birks, H.J.B., Zhong, Y., 2017. Testing the effect of the Himalayan mountains as a physical barrier to gene flow in *Hippophae tibetana* Schlect. (Elaeagnaceae). PLoS One 12, e0172948. https://doi.org/10.1371/journal.pone.0172948.
R Core Team, 2020. R: A Language and Environment for Statistical Computing. R Foundation for Statistical Computing, Vienna, Austria. https://www.R-project.org/.
Risebrobakken, B., Andersson, C., De Schepper, S., McClymont, E.L., 2016. Low-frequency Pliocene climate variability in the eastern Nordic Seas. Paleoceanography 31, 1154–1175. https://doi.org/10.1002/2015pa002918.
Rohling, E.J., Foster, G.L., Grant, K.M., Marino, G., Roberts, A.P., Tamisiea, M.E., Williams, F., 2014. Sea-level and deep-sea-temperature variability over the past 5.3 million years. Nature 508, 477. https://doi.org/10.1038/nature13230.
Salzmann, U., Dolan, A.M., Haywood, A.M., Chan, W.-L., Voss, J., Hill, D.J., Abe-Ouchi, A., Otto-Bliesner, B., Bragg, F.J., Chandler, M.A., Contoux, C., Dowsett, H.J., Jost, A., Kamae, Y., Lohmann, G., Lunt, D.J., Pickering, S.J., Pound, M.J., Ramstein, G., Rosenbloom, N.A., Sohl, L., Stepanek, C., Ueda, H., Zhang, Z., 2013. Challenges in quantifying Pliocene terrestrial warming revealed by data-model discord. Nat. Clim. Chang. 3, 969–974. https://doi.org/10.1038/nclimate2008.
Schwarz, F., Salzmann, U., Koutsodendris, A., Nie, J., Friedrich, O., Ni, J., Garzione, C., Fang, X., Wu, F., Woodward, J., Appel, E., Pross, J., 2022. Controls of precipitation and vegetation variability on the NE Tibetan Plateau during the late Pliocene warmth (~3.5–3.0 Ma). Glob. Planet. Chang. 208, 103707 https://doi.org/10.1016/j.gloplacha.2021.103707.
Seki, O., Foster, G.L., Schmidt, D.N., Mackensen, A., Kawamura, K., Pancost, R.D., 2010. Alkenone and boron-based Pliocene pCO2 records. Earth Planet. Sci. Lett. 292, 201–211. https://doi.org/10.1016/j.epsl.2010.01.037.
Seppä, H., Birks, H.J.B., Odland, A., Poska, A., Veski, S., 2004. A modern pollen–climate calibration set from northern Europe: developing and testing a tool for palaeoclimatological reconstructions. J. Biogeogr. 31, 251–267. https://doi.org/10.1111/j.1365-2699.2004.00923.x.
Shi, N., Jia-Xin, C., Königsson, L.-K., 1993. Late Cenozoic Vegetational history and the Pliocene-Pleistocene Boundary in the Yushe Basin, S. E. Shanxi, China. Grana 32, 260–271. https://doi.org/10.1080/00173139309429990.
Song, C., Dongling, G., Xiaomin, F., Zhijiu, C., Jijun, L., Shengli, Y., Hongbo, J., Burbank, D., Kirschvink, J.L., 2005a. Late Cenozoic high-resolution magnetostratigraphy in the Kunlun Pass Basin and its implications for the uplift of the northern Tibetan Plateau. Chin. Sci. Bull. 50, 1912–1922. https://doi.org/10.1360/03wd0314.
Song, M., Zhou, C., Ouyang, H., 2005b. Simulated distribution of vegetation types in response to climate change on the Tibetan Plateau. J. Veg. Sci. 16, 341–350. https://doi.org/10.1111/j.1654-1103.2005.tb02372.x.
Steph, S., Tiedemann, R., Prange, M., Groeneveld, J., Schulz, M., Timmermann, A., Nürnberg, D., Rühlemann, C., Saukel, C., Haug, G.H., 2010. Early Pliocene increase in thermohaline overturning: a precondition for the development of the modern equatorial Pacific cold tongue. Paleoceanography 25, 1–17. https://doi.org/10.1029/2008PA001645.
Stockmarr, J., 1971. Tablets with spores used in absolute pollen analysis. Pollen Spores 13, 615–621.
Su, T., Wilf, P., Xu, H., Zhou, Z.K., 2014. Miocene leaves of *Elaeagnus* (Elaeagnaceae) from the Qinghai-Tibet Plateau, its modern center of diversity and endemism. Am. J. Bot. 101, 1350–1361. https://doi.org/10.3732/ajb.1400229.
Tindall, J.C., Haywood, A.M., Salzmann, U., Dolan, A.M., Fletcher, T., 2022. The warm winter paradox in the Pliocene northern high latitudes. Clim. Past 18, 1385–1405. https://doi.org/10.5194/cp-18-1385-2022.
Tonello, M.S., Prieto, A.R., 2008. Modern vegetation–pollen–climate relationships for the Pampa grasslands of Argentina. J. Biogeogr. 35, 926–938. https://doi.org/10.1111/j.1365-2699.2007.01854.x.
Utescher, T., Bruch, A., Erdei, B., François, L., Ivanov, D., Jacques, F.M.B., Kern, A., Liu, C.Y., Mosbrugger, V., Spicer, R., 2014. The Coexistence Approach—Theoretical background and practical considerations of using plant fossils for climate quantification. Palaeogeogr. Palaeoclimatol. Palaeoecol. 410, 58–73. https://doi.org/10.1016/j.palaeo.2014.05.031.
Vincens, A., Buchet, G., Williamson, D., Taieb, M., 2005. A 23,000 yr pollen record from Lake Rukwa (8°S, SW Tanzania): New data on vegetation dynamics and climate in Central Eastern Africa. Rev. Palaeobot. Palynol. 137, 147–162. https://doi.org/10.1016/j.revpalbo.2005.06.001.
Wang, H., Ni, J., Prentice, I.C., 2011. Sensitivity of potential natural vegetation in China to projected changes in temperature, precipitation and atmospheric CO2. Reg. Environ. Chang. 11, 715–727. https://doi.org/10.1007/s10113-011-0204-2.
Wang, L., Lu, H.Y., Wu, N.Q., Li, J., Pei, Y.P., Tong, G.B., Peng, S.Z., 2006. Palynological evidence for late Miocene-Pliocene vegetation evolution recorded in the red clay sequence of the central Chinese Loess Plateau and implication for palaeoenvironmental change. Palaeogeogr. Palaeoclimatol. Palaeoecol. 241, 118–128. https://doi.org/10.1016/j.palaeo.2006.06.012.
Wang, N., Chang, M.-M., 2010. Pliocene cyprinids (*Cypriniformes*, *Teleostei*) from Kunlun Pass Basin, northeastern Tibetan Plateau and their bearings on development of water system and uplift of the area. Sci. China Earth Sci. 53, 485–500. https://doi.org/10.1007/s11430-010-0048-5.
Wang, Y., Wang, X., Xu, Y., Zhang, C., Li, Q., Tseng, Z.J., Takeuchi, G., Deng, T., 2008. Stable isotopes in fossil mammals, fish and shells from Kunlun Pass Basin, Tibetan Plateau: Paleo-climatic and paleo-elevation implications. Earth Planet. Sci. Lett. 270, 73–85. https://doi.org/10.1016/j.epsl.2008.03.006.
Wara, M.W., Ravelo, A.C., Delaney, M.L., 2005. Permanent El Niño-like Conditions during the Pliocene warm period. Science 309, 758–761. https://doi.org/10.1126/science.1112596.
Williams, M., Haywood, A.M., Harper, E.M., Johnson, A.L.A., Knowles, T., Leng, M.J., Lunt, D.J., Okamura, B., Taylor, P.D., Zalasiewicz, J., 2009. Pliocene climate and seasonality in North Atlantic shelf seas. Proc. R. Soc. A: Math. Phys. Eng. Sci. 367, 85–108. https://doi.org/10.1098/rsta.2008.0224.
Wu, F., Fang, X., Ma, Y., Herrmann, M., Mosbrugger, V., An, Z., Miao, Y., 2007. Plio–Quaternary stepwise drying of Asia: evidence from a 3-Ma pollen record from the Chinese Loess Plateau. Earth Planet. Sci. Lett. 257, 160–169. https://doi.org/10.1016/j.epsl.2007.02.029.
Wu, N., Pei, Y., Lu, H., Guo, Z., Li, F., Liu, T., 2006. Marked ecological shifts during 6.2–2.4 Ma revealed by a terrestrial molluscan record from the Chinese Red Clay Formation and implication for palaeoclimatic evolution. Palaeogeogr. Palaeoclimatol. Palaeoecol. 233, 287–299. https://doi.org/10.1016/j.palaeo.2005.10.006.
Wu, Y., Cui, Z., Liu, G., Ge, D., Yin, J., Xu, Q., Pang, Q., 2001. Quaternary geomorphological evolution of the Kunlun Pass area and uplift of the Qinghai-Xizang (Tibet) Plateau. Geomorphology 36, 203–216. https://doi.org/10.1016/S0169-555X(00)00057-X.
Yu, G., Tang, L., Yang, X., Ke, X., Harrison, S.P., 2001. Modern Pollen Samples from Alpine Vegetation on the Tibetan Plateau. Glob. Ecol. Biogeogr. 10, 503–520. https://doi.org/10.1046/j.1466-822X.2001.00258.x.
Zachos, J., Pagani, M., Sloan, L., Thomas, E., Billups, K., 2001. Trends, rhythms, and aberrations in global climate 65 Ma to present. Science 292. https://doi.org/10.1126/science.1059412.
Zhang, Y.-J., Duo, L., Pang, Y.-Z., Felde, V.A., Birks, H.H., Birks, H.J.B., 2018. Modern pollen assemblages and their relationships to vegetation and climate in the Lhasa Valley, Tibetan Plateau. China. Quat. Int. 467, 210–221. https://doi.org/10.1016/j.quaint.2018.01.040.
Zhao, Y., Yu, Z., Chen, F., Ito, E., Zhao, C., 2007. Holocene vegetation and climate history at Hurleg Lake in the Qaidam Basin, Northwest China. Rev. Palaeobot. Palynol. 145, 275–288. https://doi.org/10.1016/j.revpalbo.2006.12.002.
Zhao, Y., Liu, H., Li, F., Huang, X., Sun, J., Zhao, W., Herzschuh, U., Tang, Y., 2012. Application and limitations of the *Artemisia*/Chenopodiaceae pollen ratio in arid and semi-arid China. Holocene 22, 1385–1392. https://doi.org/10.1177/0959683612449762.